Self-Commissioning of Inverter Nonlinear Effects in AC Drives

SELF-COMMISSIONING OF INVERTER NONLINEAR EFFECTS IN AC DRIVES

I.R. Bojoi[1], *E. Armando*[1], *G. Pellegrino*[1] *and S.G. Rosu*[2],

[1]Politecnico di Torino, Italy, [2]Politehnica University of Bucharest, Romania

ABSTRACT

The paper presents a novel technique for an accurate identification of the inverter nonlinear effects, such as the dead-time and on-state voltage drops. The proposed technique is very simple and it is based only on a current control scheme. If the inverter load is an AC motor, the inverter effects can be identified at drive startup using as measured quantities the motor currents and the inverter DC link voltage. The identified inverter error is stored in a Look-Up Table (LUT) that can be subsequently used by the vector control algorithm. The proposed method has been tested on a 1 kVA inverter prototype and the obtained results demonstrate the feasibility of the proposed solution.

Index Terms— inverter nonlinearity, self-commissioning, current control, AC drives

1. INTRODUCTION

The continuous need for energy saving induced the need for more efficient electrical drives. The research work has focused on more efficient AC machines and also on optimal control techniques able to fully exploit the machine features. Moreover, in many applications sensorless control techniques have been introduced, leading to a cost reduction and to increased reliability compared with the drives that use mechanical position sensors [1-7].

While the induction motor is still a valid solution for many applications, the use of synchronous machines like the Surface Mounted Permanent Magnet (SMPM) and Internal Permanent Magnet (IPM) have been expanded to applications like automotive, home appliances and power generation. Independently on the adopted motor solution, the inverter influence on the control scheme is represented by the distortion of the inverter output voltage due to the dead-effects. In case of sensorless drives, this distortion usually causes a non-optimal motor exploitation at low speed operation due to an error in the estimated position of the adopted reference frame used by the motor control scheme. In addition, the motor currents will be distorted, resulting in unnecessary torque ripple. The low speed is intended as the speed range where the voltage drop on the machine resistance cannot be neglected with respect to the machine back-EMF.

The literature reports many papers describing the inverter nonlinear behavior and its influence on sensorless control of AC machines [1-18], as well as compensation schemes. Most of the papers consider the inverter influence as a pole voltage error that depends on the sign of the pole current, suggesting that the inverter error can be modeled as sign function of the phase current [1-9].

A more detailed analysis presented in [11] demonstrated that the pole voltage error depends also on the pole current at low current values, due to the power devices parasitic capacitances. An analytical technique based on power devices datasheet has been presented in [18] to get the voltage error. However, the power devices parameters may change respect to the data sheet and due to the temperature variation.

For this reason, a self-commissioning solution, able to obtain the inverter pole voltage error according the phase current is preferred. The solutions presented in the literature are based on harmonic analysis of currents in synchronous reference frame [10], repetitive control [15,16] or on the flux observer used for motor flux estimation, as in [17].

The inverter self-commissioning algorithm proposed in this paper does not depend on the machine type and needs only a roughly tuned current control scheme using normal current measurement techniques employed by low-cost systems. The procedure is executed with the motor at standstill, or even with a three-phase passive Resistive-Inductive (RL) load if the inverter commissioning is performed without having the target motor available. The inverter pole voltage error is mapped in a Look-Up Table (LUT) having as input the phase current.

The paper is organized as follows. The inverter nonlinear effects are briefly analyzed in Section II. The detailed description of the self-commissioning procedure is performed in Section III. Experimental results obtained for a 1 kVA inverter prototype are presented in Section IV to validate the proposed solution.

2. INVERTER NONLINEAR EFFECTS

The inverter modeling has been analyzed in many papers, with the aim at describing and compensating the voltage error between the command voltage and the actual motor voltage. As already known, this voltage error is produced by the following sources:

(1) inverter dead-time;

(2) on-state voltage drops on the power switches.

A. Dead-time voltage error

As demonstrated in the literature [7], the dead-time voltage vector error is

$$\bar{v}_{dt} = \frac{4}{3} \cdot t_d \cdot f_s \cdot V_{dc} \cdot sign(\bar{i}) \quad (1)$$

where V_{dc} is the inverter DC link voltage, f_s is the switching frequency and t_d is the dead-time as the time interval between the off state and on state of two controllable power switches belonging to the same inverter leg.

The nonlinear term in (1) is the vector signum of the inverter load currents defined as [7]

$$sign(\bar{i}) = \frac{1}{2} \cdot \left[sign(i_a) + e^{j(2\pi/3)} \cdot sign(i_b) + e^{j(4\pi/3)} \cdot sign(i_c) \right] \quad (2)$$

where i_a, i_b and i_c are the motor phase currents.

The $sign(\bar{i})$ vector is an unity vector that has six positions in the stationary (α,β) frame that from a hexagon. The $sign(\bar{i})$ vector position is the closest dot to the current vector position within a range of ±30 electrical degrees, as the example shown in Fig.1.

Defining a (*d*,*q*) reference frame with the *d*-axis aligned with the load current vector (Fig.1) that rotates with the electrical speed, the (*d*,*q*) components of the signum current vector are shown in Fig.2 with respect to the position ϑ of the current vector $\bar{i}$.

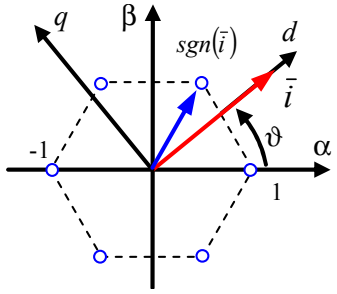

Fig. 1. Load current vector $\bar{i}$ and signum current vector along with its six possible positions.

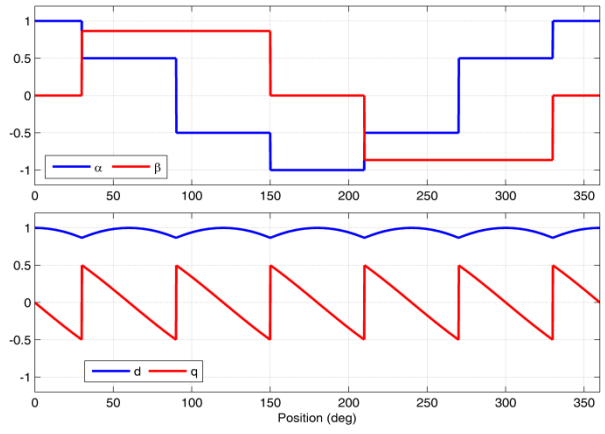

Fig. 2. (α,β) components (top) and (*d*,*q*) components (bottom) of the signum current vector.

From Fig.2, it results that the voltage error caused by the dead-time effects and computed with (1) has two components in stator current frame. The direct component introduce fundamental voltage error, while the quadrature component has zero mean value and produces only distortion at six times the fundamental frequency.

B. Voltage error caused by on-state voltage drops

As shown in the literature [7], for small inverter output voltages (duty-cycles around 0.5), the voltage error vector due to the on-state voltage drops can be written as

$$\bar{v}_{on} = \frac{4}{3} \cdot V_{th} \cdot sign(\bar{i}) + R_d \cdot \bar{i} \quad (3)$$

where the threshold voltage V_{th} and the equivalent dynamic resistance R_d are computed as

$$\begin{cases} V_{th} = \dfrac{V_{th,sw} + V_{th,fw}}{2} \\ R_d = \dfrac{R_{sw} + R_{fw}}{2} \end{cases} \quad (4)$$

where subscript '*sw*' stands for active switch (e.g. IGBT) while the subscript '*fw*' stands for freewheeling diode.

It can be clearly seen from (3) that the voltage error contains one nonlinear term that is similar with the voltage error caused by the dead-time, while the other term is a linear voltage drop.

C. Overall inverter voltage error

According to (1) and (3), the overall inverter voltage error vector is

$$\bar{v}_{err} = \frac{4}{3} \cdot V_{th}' \cdot sign(\bar{i}) + R_d \cdot \bar{i} \quad (5)$$

where $V_{th}' = V_{th} + t_d \cdot f_s \cdot V_{dc}$.

The inverter nonlinear effects is represented by the equivalent term V_{th}' that includes both dead-time and on-state threshold voltage.

While the voltage error vector (5) represents properly the inverter behavior at high load current levels, the situation changes significantly for low current levels. As shown in [11,18], at low current levels the power switches turn-off time increases dramatically. That is equivalent to a reduction of the term V_{th}' in (5). A comprehensive modeling of the inverter behavior at low current levels is reported in [11,18].

The inverter error identification aims at obtaining the voltage error (5) with a simple self-commissioning procedure without using power switches data sheet [18] or other complicated algorithms [15,16].

According to (5), the inverter voltage vector contains one linear term that can be seen as an additional resistance R_d that must added to the load resistance. For this reason, the proposed algorithm gets first the total resistance. Then the

nonlinear pole voltage error is obtained, as described in detail in the next section.

3. IDENTIFICATION OF THE INVERTER ERROR

The employed control scheme for inverter self-commissioning is shown in Fig. 3. The inverter load can be any kind of three-phase motor (induction, PM, IPM) compatible with the inverter rated power, but the proposed algorithm can be tested also with a three-phase RL load as well.

The control uses a conventional current control scheme implemented in a rotating (*d,q*) frame. If the position used for direct and inverse transformations is equal to zero, then the imposed current vector is aligned on the α-axis in stationary reference frame, since the reference *q*-axis component is also set to zero, as shown in Fig.3. As consequence, the reference current on *d*-axis will be the magnitude of the current vector I_{test} imposed to the motor along the α-axis that also coincides with the motor phase *a*-axis. In this case, $i_a>0$, $i_b<0$, $i_c<0$ and the sign current vector and the corresponding inverter voltage vector are

$$sign(\bar{i}) = \frac{1}{2}\cdot\left[1 - e^{j(2\pi/3)} - e^{j(4\pi/3)}\right] = 1 + j0 \qquad (6)$$

$$\bar{v}_{err} = v_{err,\alpha} + j0 = \frac{4}{3}\cdot V_{th}^{'} + R_d \cdot i_\alpha = v_{err,\alpha} \qquad (7)$$

As described above, the inverter identification is performed using two different steps.

A. Step 1: Evaluation of the overall resistance R_d+R_s

For motor currents that are high enough, the nonlinear term of (7) does not depend on the current value, if the DC link voltage does not change. This property can be used by generating two different constant current levels I_{test1} and I_{test2} along α-axis, as shown in Fig.4. If the load is a PM machine or an IPM machine, then an initial parking current must be used to park the rotor along the α-axis. The time length of the parking pulse must be high enough to avoid any rotor oscillations.

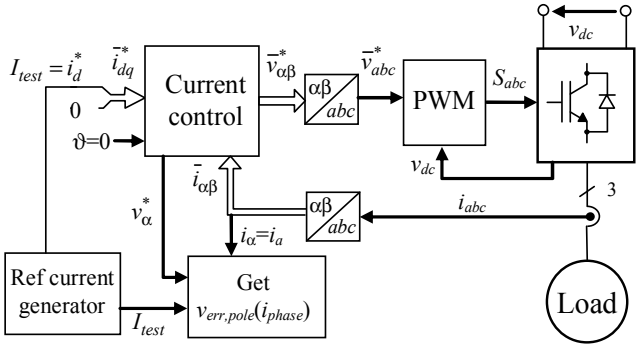

Fig. 3. Control scheme for inverter self-commissioning.

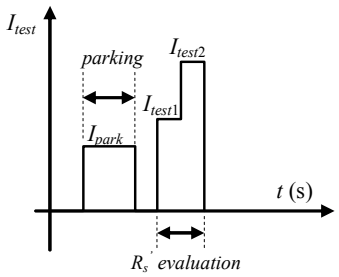

Fig. 4. Current profile for overall resistance evaluation.

If the load is an induction machine or a synchronous machine with the rotor parked along the α-axis, then the motor operation is DC and no torque is produced. As result, the rotor speed is zero and the entire voltage generated along α-axis will be applied to the overall resistance R_d+R_s.

Taking into account the inverter error, the reference voltage generated by the current control on α-axis at DC steady-state operation is

$$V_\alpha^* = \frac{4}{3}\cdot V_{th}^{'} + \left(R_d + R_s\right)\cdot I_\alpha \qquad (8)$$

Assuming the same nonlinear term for the two current steps, then the overall resistance can be obtained as

$$R_d + R_s = R_s^{'} = \frac{\Delta V_\alpha^*}{\Delta I_{test}} = \frac{V_{\alpha,2}^* - V_{\alpha,1}^*}{I_{test2} - I_{test1}} \qquad (9)$$

The time length for the two current steps must be high enough to get steady-state DC operation. The voltages used in (9) can be sampled at the end of each current pulse.

The values used for I_{test1} and I_{test2} must be chosen to be similar with the machine rated peak current. The overall resistance in (9) is accurate only if the DC link voltage does not change during the two current steps.

B. Step 2: Evaluation of the pole error voltage

The pole error voltage is obtained as a Look-Up Table (LUT) whose input is the phase current that is in a range between 0 and a maximum value $I_{test,LUT}$. The LUT is obtained by imposing a staircase current in the α-axis using a specified number of steps, as shown in Fig. 5.

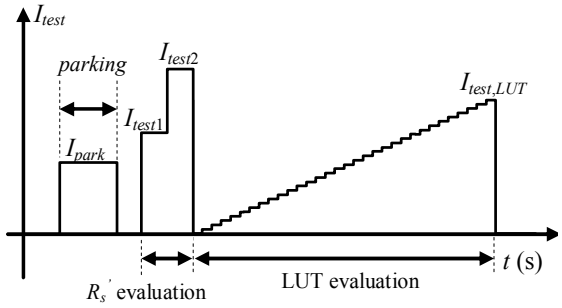

Fig. 5. Complete current profile for inverter identification.

The time length of one current step should be chosen to get DC steady-state operation. At the end of each current step k, the reference voltage on the α-axis will be

$$V_{\alpha}^{*}(k)=\frac{4}{3}\cdot V_{th}^{'}+R_{s}^{'}\cdot I_{\alpha}(k) \qquad (10)$$

Assuming a constant overall resistance that is detected using (9), then the pole voltage error for the k^{th} current step is

$$V_{err,pole}(k)=\frac{3}{4}\cdot\left[V_{\alpha}^{*}(k)-R_{s}^{'}\cdot I_{\alpha}(k)\right] \qquad (11)$$

The LUT can be built by storing the pole error voltage, the maximum test current and the step number.

Since the inverter pole voltage error is symmetrical for both positive and negative values of the load current [18], only the positive load current case suffices for a complete characterization of this error.

4. EXPERIMENTAL RESULTS

The experimental tests have been performed with an 1 kVA IGBT inverter prototype based on the ST Microelectronics STGIPL14K60 power module (described in Appendix) that uses 1 µs of dead-time and a switching frequency of 16 kHz. The inverter test setup is shown in Fig. 6. The inverter DC link is fed by a regulated DC voltage supply, while the inverter load is an induction motor. described in Appendix. The DC link voltage supply allows keeping a constant DC link voltage during the inverter self-commissioning test. The whole identification control algorithm has been implemented on a Texas Instruments control card with the TMS320F28069 microcontroller. The control sampling frequency has been set at 16 kHz.

The current measurement has been done using shunts mounted between the IGBTs emitters and the negative DC link rail, as for low cost systems. The phase currents have been evaluated by synchronous sampling with the underflow condition of the timer used as time base for the PWM generation units of the microcontroller.

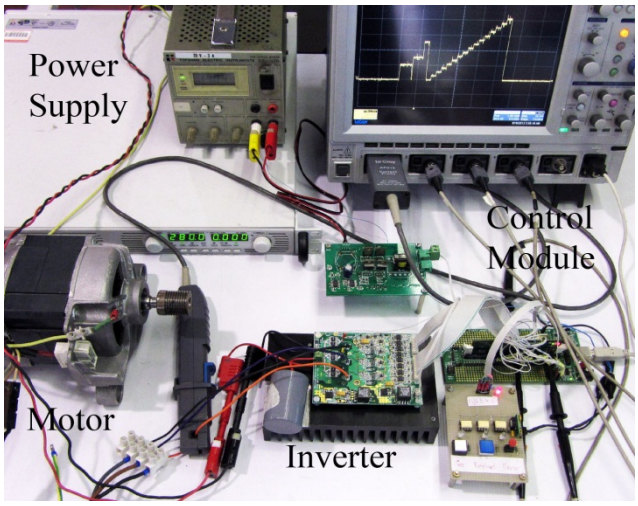

Fig. 6. Inverter test setup.

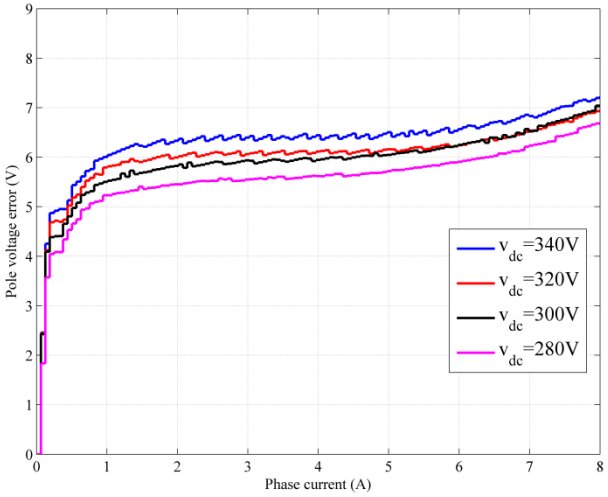

Fig. 7. Pole error voltage LUT using 128 points, $I_{test,LUT}$=8A and different DC link voltages. Dead-time is 1 µs.

The inverter identification test has been performed first up to the maximum motor current of 8A using 128 points. The time length for one current step has been set at 250 ms.

The LUT pole error voltage obtained for different DC link voltage values is shown in Fig. 7.

The results from Fig. 7 may lead to a wrong conclusion regarding an increase of the voltage error for high current values. The pole voltage error increase is not caused by the inverter, but by an increase of the stator resistance due to the motor heating at high current values. To demonstrate this statement, the test has been repeated, but using only 16 points for the LUT. In this case, the time length for the test is significantly shorted (4 seconds compared with 32 seconds for 128 points LUT) and the stator resistance will not change. The results are shown in Fig.8, along with the voltage error obtained for a DC link voltage of 340V and 128 points used for comparison.

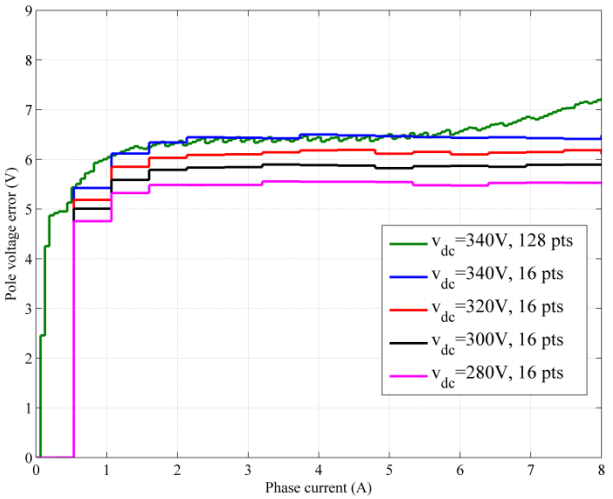

Fig. 8. Pole error voltage LUT using 128 points and 16 points, $I_{test,LUT}$=8A and different DC link voltages. Dead-time is 1 µs.

The results from Fig. 8 clearly demonstrate that above 3A the voltage error is a flat curve, i.e. the equivalent term $V_{th}^{'}$ from (5) becomes constant. As a consequence, the inverter pole voltage should be obtained only between 0 and 3A, using a proper LUT resolution.

The final pole error voltage identification has been performed using 64 points LUT up to 3A of phase current. The motor phase current i_a during the identification is shown in Fig.9. The current steps I_{test1} and I_{test2} used for the overall resistance identification were 3A and 5A, respectively. Although the motor used for the test was an induction machine, the implemented algorithm used an initial current step of 2A that was normally used for rotor parking of a PM machine, as described in Fig. 5.

The pole voltage errors resulted from the identification are shown in Fig. 10. The obtained LUT can be used to get the inverter error voltage vector in stationary frame, as shown in Fig. 11.

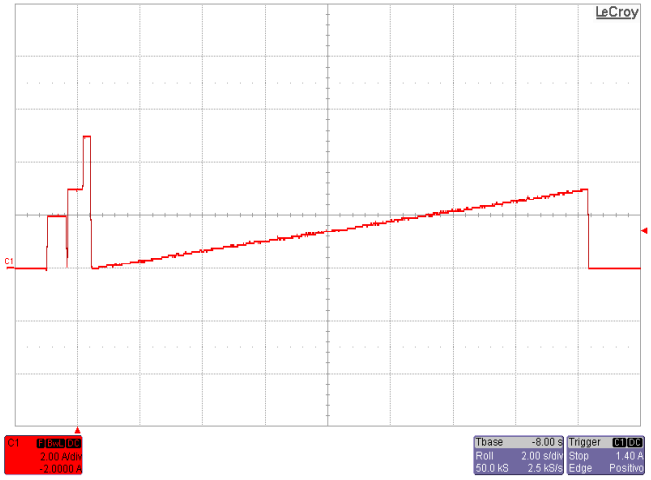

Fig. 9. Motor phase current i_a (2A/div) during the inverter identification using 3A and 64 points LUT.

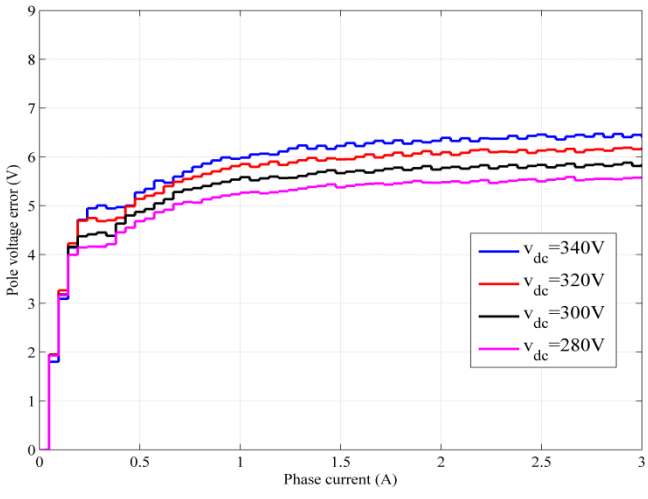

Fig. 10. Pole error voltage LUT using 64 points, $I_{test,LUT}$=3A and different DC link voltages. Dead-time is 1 µs.

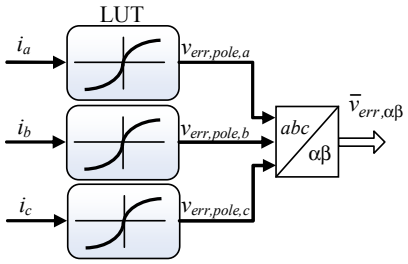

Fig. 11. Inverter voltage error vector computation in stationary frame.

The acquired phase currents are used to get the individual phase pole voltage errors, that are symmetrical for both positive and negative current values. The computed inverter voltage error $\bar{v}_{err}$ can be used by the motor control algorithm to correctly estimate the voltage delivered to the motor.

The proposed algorithm has been tested also for different values of the dead-time and the results are shown in Fig.12 for a DC link voltage of 340V. As expected, the voltage error proportionally increases with the dead-time.

5. CONCLUSIONS

The paper presents a simple self-commissioning algorithm for the identification of the inverter nonlinear effects in AC drives. When compared to previous solutions from the literature, the proposed self-commissioning algorithm does not depend on the adopted vector control technique and needs only a current control scheme based on a normal current measurement procedure used for low cost systems. The proposed procedure is implemented with the motor at standstill before the drive startup. The identification procedure obtains the inverter pole error voltage as a LUT having as input the phase current, with no need of complex computations or power devices datasheet parameters. Experimental results for an 1 kVA inverter prototype are provided to validate the proposed solution.

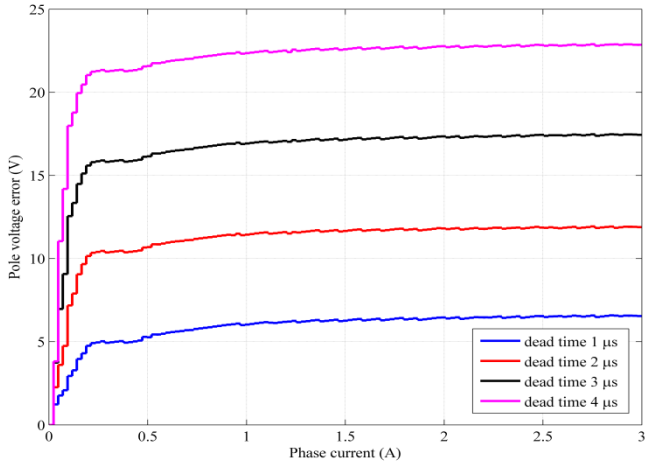

Fig. 12. Pole voltage error LUT at 340V for different values of the dead-time.

6. APPENDIX

The STGIPL14K60 is a 600V, 15A, Intelligent Power Module (IPM) that contains a three-phase IGBT inverter with internal drivers and operational amplifiers for current sensing using bottom side shunts.
The motor is a 700 W, 195V/60Hz, 3A, 2-poles, three-phase induction machine built for home appliances.

7. ACKNOWLEDGMENT

This work has been partially funded by the Sectoral Operational Programme Human Resources Development 2007-2013 of the Romanian Ministry of Labour, Family and Social Protection through the Financial Agreement POSDRU/88/1.5/S/61178.

8. REFERENCES

[1] J. Choi and S. Sul, "Inverter Output Voltage Synthesis Using Novel Dead Time Compensation," *IEEE Trans. Power Electron*., vol. 11, no. 2, pp. 221–227, Mar. 1996.

[2] R. Sepe and J. Lang, "Inverter nonlinearities and discrete-time vector current control," *IEEE Trans. Ind. Appl.*, vol. 30, no. 1, pp. 62–70, Jan./Feb. 1994.

[3] K. D. Hurst, T. G. Habetler, G. Griva, and F. Profumo, "Zero-Speed Tacholess IM Torque Control: Simply a Matter of Stator Voltage Integration," *IEEE Trans. Ind. Appl.*, vol. 34, no. 4, pp. 790–795, Jul./Aug. 1998.

[4] C. Attaianese and G. Tomasso, "Predictive Compensation of Dead-Time Effects in VSI Feeding Induction Motors," *IEEE Trans. Ind. Appl.*, vol. 37, no.3, May/June 2001, pp. 856–863.

[5] J. Holtz, "Sensorless control of induction motor drives," *Proc. IEEE,* vol. 90, no. 8, pp. 1359–1394, Aug. 2002.

[6] D. Casadei, G. Serra, A. Tani, L. Zarri, and F. Profumo, "Performance Analysis of a Speed-Sensorless Induction Motor Drive Based on a Constant-Switching-Frequency DTC Scheme," *IEEE Trans. Ind. Appl.*, vol.39, no.2, March/April 2003, pp. 476–484.

[7] J. Holtz and J. Quan, "Sensorless Vector Control of Induction Motors at Very Low Speed Using a Nonlinear Inverter Model and Parameter Identification," *IEEE Trans. Ind. Appl.*, vol. 38, no. 4, pp. 1087–1095, Jul./Aug. 2002.

[8] J. Guerrero, M. Leetmaa, F. Briz, A. Zamarron, and R. Lorenz, "Inverter Nonlinearity Effects in High-Frequency Signal-Injection-Based Sensorless Control Methods," *IEEE Trans. Ind. Appl.*, vol. 41, no. 2, pp. 618–626, Mar./Apr. 2005.

[9] J. K. Pedersen, F. Blaabjerg, J. W. Jensen, and P. Thogersen, "An Ideal PWM-VSI Inverter with Feedforward and Feedback Compensation," in *Conf. Rec. EPE*, 1993, pp. 501–507.

[10] H. Zhao, Q.M. Jonathan Wu, and A. Kawamura, "An Accurate Approach of Nonlinearity Compensation for VSI Inverter Output Voltage," *IEEE Trans. Power Electron*., vol.19, no.4, July 2004, pp. 1029–1035.

[11] N. Urasaki, T. Senjyu, T. Kinjo, T. Funabashi, and H. Sekine, "Dead-time compensation strategy for permanent magnet synchronous motor drive taking zero-current clamp and parasitic capacitance effects into account," *IEE Proc. Electr. Power Appl*., vol.152, no.4, July 2005, pp.845–853.

[12] T.J. Summers and R.E. Betz, "Dead-Time Issues in Predictive Current Control," *IEEE Trans. Ind. Appl.*, vol. 40, no.3, May/June 2004, pp. 835–844.

[13] L. Ben-Brahim, "On the Compensation of Dead Time and Zero-Current Crossing for a PWM-Inverter-Controlled AC Servo Drive," *IEEE Trans. Ind. Electron*., vol. 51, no. 5, Oct. 2004, pp. 1113-1117.

[14] L. Chen and F.Z. Peng, "Dead-Time Elimination for Voltage Source Inverters," *IEEE Trans. Power Electron*., vol. 23, no. 2, March 2008, pp.574–580.

[15] S. Bolognani and M. Zigliotto, "Self-commissioning compensation of inverter non-idealities for sensorless AC drives applications," in *Proc. IEE Power Electron*., Mach. Drives, 2002, pp. 30–37.

[16] S. Bolognani, L. Peretti, and M. Zigliotto, "Repetitive-Control-Based Self-Commissioning Procedure for Inverter Nonidealities Compensation," *IEEE Trans. Ind. Appl*., vol. 44, no. 5, pp. 1587–1596, Sep./Oct. 2008.

[17] G. Pellegrino, I.R. Bojoi, P. Guglielmi, and F. Cupertino, "Accurate Inverter Error Compensation and Related Self-Commissioning Scheme in Sensorless Induction Motor Drives," *IEEE Trans. Ind. Appl.*, vol. 46, no.5, Sept./Oct. 2010, pp. 1970–1978.

[18] D.E. Salt, D. Drury, D. Holliday, A. Griffo, P. Sangha, and A. Dinu, "Compensation of Inverter Nonlinear Distortion Effects for Signal – Injection-Based Sensorless Control," *IEEE Trans. Ind. Appl.*, vol. 47, no.5, Sept./Oct. 2011, pp. 2084–2092.